Impact of land convection on troposphere-stratosphere exchange in the tropics

P. Ricaud, Brice Barret, Jean-Luc Attié, E. Le Flochmoën, Erwan Motte, H. Teyssèdre, V.-H. Peuch, N. Livesey, A. Lambert, Jean-Pierre Pommereau

Atmos. Chem. Phys. Discuss., 7, 3269–3300, 2007
www.atmos-chem-phys-discuss.net/7/3269/2007/

Atmospheric Chemistry and Physics Discussions

Impact of land convection on troposphere-stratosphere exchange in the tropics

P. Ricaud[1], B. Barret[1], J.-L. Attié[1], E. Le Flochmoën[1], E. Motte[1], H. Teyssèdre[2], V.-H. Peuch[2], N. Livesey[3], A. Lambert[3], and J.-P. Pommereau[4]

[1]Laboratoire d'Aérologie, CNRS, Université de Toulouse III, Toulouse, France
[2]Centre National de Recherche Météorologique, Météo-France, Toulouse, France
[3]NASA Jet Propulsion Laboratory, Pasadena, California, USA
[4]CNRS, Service d'Aéronomie, Verrières-le-Buisson, France

Received: 7 February 2007 – Accepted: 25 February 2007 – Published: 1 March 2007

Correspondence to: P. Ricaud (philippe.ricaud@aero.obs-mip.fr)

Abstract

The mechanism of troposphere-stratosphere exchange in the tropics was investigated from space-borne observations of the horizontal distributions of nitrous oxide (N_2O), methane (CH_4) and carbon monoxide (CO) at 17 km in March-April-May by the ODIN/Sub-Millimeter Radiometer (SMR), the Upper Atmosphere Research Satellite (UARS)/Halogen Occultation Experiment (HALOE) and the TERRA/Measurements Of Pollution In The Troposphere (MOPITT) instruments in 2002–2004, completed by recent observations of the AURA/Microwave Limb Sounder (MLS) instrument during the same season in 2005. At the top of the Tropical Tropopause Layer (TTL), all gases show significant longitudinal gradients with maximum amounts primarily over Africa and, depending on the species, secondary more or less pronounced maxima above northern South America and South-East Asia. The Maritime continent in the Western Pacific never appears as a source region for the stratosphere. The large longitudinal gradient at latitudes where the circulation is essentially zonal, and the co-location of the maximum tropospheric trace gases concentrations with the overshooting features reported by the Tropical Rainfall Measuring Mission (TRMM) satellite precipitation radar, strongly supports that rapid uplift over land convective regions is the dominating process of troposphere-stratosphere exchange. Calculations carried out with the MOCAGE-Climat chemical transport model well capture the location of the maximum gas concentration in the TTL but of lesser amplitude. Although there are obvious misrepresentations of some of the sources in the model, i.e. CH_4 emissions by evergreen forests, the main reason for discrepancy appears to be the underestimation of the maximum altitude reached by land convective transport in MOCAGE.

1 Introduction

The Upper Troposphere-Lower Stratosphere (UTLS) is the atmospheric layer where dynamical, chemical and radiative processes strongly interact to control the atmo-

ACPD

7, 3269–3300, 2007

spheric composition and its impact on climate change. The general characteristics of dynamical processes controlling the UTLS were described in Holton et al. (1995). Air masses brought into the upper troposphere by convection in the tropics enter the lower stratosphere from where they are distributed at global scale by the Brewer-Dobson circulation. The still open question is how air masses are transported from the upper troposphere into the lower stratosphere across the Tropical Tropopause or Tropical Transition Layer (TTL), the region of intermediate lapse rate extending from the level of zero net radiative heating (∼14 km, ∼150 hPa) to the level of stratospheric lapse rate (∼19 km, ∼70 hPa). Two mechanisms are actually proposed: convection up to the base of the TTL around 14 km followed by a slow uplift by radiative heating (Sherwood and Dessler, 2000) or fast convective overshooting predominantly above continental areas (Danielsen, 1982). Although the existence of the second mechanism is generally accepted (Danielsen, 1993), the aim is to know its importance at global scale, thought to be generally limited because of the lower cloud-top altitude over land areas displayed by the Outgoing Longwave Radiation (OLR) satellite images, compared to that over the Maritime Continent in the Western Pacific. However, as shown by Alcala and Dessler (2002) from comparisons between thermal imagery and precipitation radar measurements from the Tropical Rainfall Measuring Mission (TRMM) satellite, the OLR is not a good indicator of cloud penetration in the stratosphere. In contrast to what is generally accepted, the radar indicates higher and more frequent Overshooting Precipitation Features (OPF) above land areas (Liu and Zipser, 2005) with a marked diurnal variation peaking at local afternoon. This picture is consistent with the maximum lightning flashes seen by the Optical Transient Detector instrument onboard the MicroLab-1 satellite, indicative of the updraft velocity near the tropopause (Christian et al., 2003). According to those results, the maximum penetration of convective systems in the lower stratosphere would occur primarily in Africa at all seasons, then in South America in the Austral summer or Central America in the Northern summer, and to a much more limited extent, over South-East Asia and the Indonesian Islands in the Northern summer and Northern Australia in the Austral summer.

The method proposed here for studying the relative importance of slow radiative heating compared to fast convective troposphere-stratosphere exchange at global scale is to look at the horizontal distributions of trace gases of tropospheric origin, in the TTL and the lower stratosphere. Indeed, if slow ascent induced by radiative heating dominates, transport through the tropopause will not be constrained to any particular location and no variation in the zonal distribution of tropospheric species is expected in the lower stratosphere, as concluded by Levine et al. (2007). In contrast, if fast convective overshooting (hours) dominates compared to the 3–4 weeks required for an air mass to circumnavigate in the TTL, the concentration of tropospheric trace gases should display marked maxima above overshooting areas, possibly modulated by the intensity of the source at surface level.

Here, the relative importance of the mechanisms of troposphere-stratosphere exchange is diagnosed from space-borne observations of the horizontal distribution of nitrous oxide (N_2O) from the ODIN/Sub-Millimeter Radiometer (SMR) and the AURA/Microwave Limb Sounder (MLS) instruments, methane (CH_4) from the Upper Atmosphere Research Satellite (UARS)/Halogen Occultation Experiment (HALOE) instrument and carbon monoxide (CO) from the TERRA/Measurements Of Pollution In The Troposphere (MOPITT) and the AURA/MLS instruments. Indeed, stratospheric N_2O and CH_4 are excellent tracers of dynamical processes since their sources are located at the surface (soils, wetlands, biomass burning, industrial exhausts, ...), and their sinks are essentially in the stratosphere through photolysis and chemical reactions with electronically-excited oxygen atoms and OH, respectively (Brasseur et al., 1999). Consequently, their photochemical lifetimes varies from about a century (N_2O) or a decade (CH_4) in the troposphere to less than one year in the middle stratosphere. With a shorter lifetime, CO is a good tracer of pollution either from industrial exhaust or from biomass burning. Its tropospheric lifetime of the order of one month enables to trace long-range transport of pollution in the horizontal direction within the free troposphere (e.g. Heald et al., 2003) and in the vertical direction through the UTLS (e.g. Li et al., 2005). Consequently, CO distribution can help characterizing the seasonal changes in

convective outflow (Folkins et al., 2006), and in biomass burning via the detection of the carbon monoxide tape recorder in the stratosphere (Schoeberl et al., 2006).

Here we focus on the Northern Hemisphere Spring period in March-April-May (MAM), the season of the circumnavigating long duration balloon flights of the HIBISCUS project in the tropics (Pommereau et al., 2007). The study is based upon the measurements of N_2O, CH_4, and CO by space-borne sensors and related products (OLR, fire counts, potential temperature, winds, temperature and vertical flux) over the three consecutive years: 2002, 2003 and 2004. The observed distributions of these species are compared to simulations of the three-dimensional (3-D) Chemical Transport Model (CTM) MOCAGE (Modèle de Chimie Atmosphérique à Grande Echelle) covering both the troposphere and the stratosphere. The paper is organized as follows. Section 2 provides a description of the satellite measurements. The resulting distributions of the species in the TTL are analysed and discussed together with meteorological information in Sect. 3. The results of model simulations are compared to the observations in Sect. 4, together with a discussion on the distribution of sources at the surface and on the convection intensity in the model.

2 Satellite data

The following section provides the information on the trace gas measurements performed by the ODIN/SMR, UARS/HALOE, TERRA/MOPITT and AURA/MLS space-borne sensors, together with information related to OLR measurements from the National Oceanic and Atmospheric Administration (NOAA) Advanced Very High Resolution Radiometer (AVHRR) sensors, and to fire count measurements from the Visible and IR Scanner (VIRS) instrument onboard TRMM.

2.1 ODIN/SMR N_2O

The ODIN mini-satellite is a Swedish-led project funded jointly by Sweden, Canada, France, and Finland (Murtagh et al., 2002). It was placed into a 600-km Sun-synchronous, terminator orbit by a START-1 rocket on 20 February 2001, and is still operational. Observing times are equally shared between astronomy and aeronomy. ODIN includes the SMR microwave instrument (Frisk et al., 2003) that can measure ozone (O_3), chlorine monoxide (ClO), N_2O, nitric acid (HNO_3), water vapour (H_2O), and CO in the frequency domain 480–580 GHz. Most of the measurements have been validated (e.g. Barret et al., 2006). The present study is based upon the retrievals of the 502.296-GHz N_2O line measured by Odin/SMR using the Optimal Estimation Method (Rodgers, 2000). On average, measurements of N_2O are performed one day out of three. In our analysis, we have restricted the N_2O data set to measurement response greater than 0.75, i.e. with a minor contribution from a climatology of N_2O used as a priori. All the measurements performed during the period March-May 2002, 2003 and 2004 have been analysed in version V222 (Urban et al., 2005). The vertical resolution is 2 km. Only the lowermost layer at 17 km where meaningful information can be retrieved is considered in the present study. The single scan precision is ranging from 10 to 45 ppbv for N_2O mixing ratios ranging from 0 to 325 ppbv. The total systematic error is from 3 to 35 ppbv for N_2O mixing ratios from 0 to >150 ppbv. Measurements have been averaged into bins of 10° latitude × 30° longitude.

2.2 UARS/HALOE CH_4

The HALOE instrument onboard the UARS satellite measured CH_4 from October 1991 to November 2005 (Russell et al., 1993). Since measurements are performed using the solar occultation technique, profiles are continuously retrieved in the tropical region. Sensitivity of the CH_4 measurements generally allows observations around the tropopause. As for Odin, data have been averaged into bins of 10° latitude × 30° longitude and linearly interpolated onto the 17-km altitude layer. This corresponds to 2–10

vertical profiles available per bin in the equatorial region from 100 to 60 hPa during the period MAM 2002–2004. For the analysis presented here, only profiles with error uncertainties less than 100% have been included. In addition, as suggested in Park et al. (2004), we have only considered CH_4 mixing ratios less than 3 ppmv. The total error for individual profiles of CH_4 is 20% (Park et al., 2004) in the 50–100 hPa domain and the vertical resolution is ~2–3 km.

2.3 TERRA/MOPITT CO

The TERRA/MOPITT instrument (Drummond and Mand, 1996) has been monitoring global tropospheric CO from March 2000 to date. These data have been intensively validated (see e.g. Barret et al., 2003; Emmons et al., 2004 and 2007[1]). The pixel size is 22 km×22 km and the vertical profiles are retrieved on 7 pressure levels (surface, 850, 700, 500, 350, 250 and 150 hPa). The maximum likelihood method, used to retrieve the MOPITT CO, is a statistical combination of the measurements and a priori information (Rodgers, 2000). The retrieval profiles are characterized by their averaging kernels which give information on the vertical resolution of the measurements. In particular, the Degree of Freedom for Signal (DFS), which is the trace of the averaging kernel matrix, indicates the number of independent pieces of information contained in the measurements. It depends, via the surface temperature, on the latitude and the alternating day/night. During daytime over the tropics, the zonal average DFS is about 1.5 (Deeter et al., 2004); this insures that MOPITT provides almost two independent pieces of information located in the lower and in the upper troposphere. Furthermore, in this study, we only consider daytime MOPITT CO (Version 3) retrievals at 850 and 150 hPa with less than 40% a priori contamination to insure a consistent and good quality of the dataset. In addition, MOPITT CO data have been averaged within bins of

[1] Emmons, L. K., Pfister, G. G., Edwards, D. P., Gille, J. C., Sachse, G., Blake, D., Wofsy, S., Gerbig, C., Matross, D., and Nédélec, P.: MOPITT validation exercises during Summer 2004 field campaigns over North America, J. Geophys. Res., special issue ICARTT, submitted, 2007.

0.5°×0.5°.

2.4 AURA/MLS N_2O and CO

The MLS sounder is one of the four instruments onboard the Earth Observing System (EOS) AURA satellite launched on 15 July 2004 in a Sun-synchronous orbit (98° inclination) at ~705 km altitude with an ascending node at 13:45 hours (local time). Vertical profiles of 17 target atmospheric parameters, among which 14 trace gases, are retrieved from the MLS observations with a 165-km horizontal spacing along the orbit track (Waters et al., 2006). The retrieval methodology for the MLS observations, based on the Optimal Estimation Method, is described in detail in Livesey et al. (2006). The new concept implemented in the MLS retrieval algorithm is a 2-D approach allowing retrieval of atmospheric structures in both the vertical and line of sight directions taking into account the overlapping regions covered by consecutive scans. A detailed description of the characteristics of the version 1.5 MLS products used in the present study can be found in the "EOS MLS Version 1.5 Level 2 data quality and description document" (Livesey et al., 2005). First results from CO measured by MLS are described in Filipiak et al. (2005). CO profiles are retrieved with a single-scan precision of ~30 ppbv and a vertical resolution of ~4 km in the upper troposphere and lower stratosphere. The N_2O retrievals are considered useful from 100 to 1 hPa with a vertical resolution of ~4 km. An estimated precision of ~30 ppbv is reported at the 100 hPa level in Froidevaux et al. (2006). MLS N_2O and CO data have been averaged within bins of 10° latitude × 30° longitude.

2.5 NOAA/AVHRR OLR

OLR is measured by the NOAA/AVHRR sensors. Interpolated data (Liebmann and Smith, 1996) are taken from the NOAA-CIRES Climate Diagnostics Centre web site http://www.cdc.noaa.gov, from the NOAA 16 series of satellites. Data are binned within boxes of 2.5° latitude × 2.5° longitude. The OLR is a measure of the thermal infrared

radiation that escapes from the top of the Earth's atmosphere back into space. Cumulonimbus clouds, representative of deep convection, have high and cold tops and they radiate little longwave radiation to outer space. Regions with low OLR are therefore associated with deep convection. OLR data have been averaged over the MAM 2002–2004 period. Areas of OLR with values less than 236 and 220 W m^{-2} can be considered as an estimation of the convective outflow location in the middle (~400 hPa) and in the upper (~100 hPa) tropical troposphere, respectively.

2.6 TRMM/VIRS fire counts

The location of fire counts is estimated from the measurements of the VIRS instrument onboard TRMM. The VIRS is a 5-channel cross-track scanning radiometer that measures radiance in five bandwidths from the visible through the infrared spectral regions: 0.63, 1.6, 3.75, 10.80, and 12.0 μm at 2 km horizontal resolution (Giglio et al., 2000). Although the VIRS instrument is designed primarily to study clouds and precipitation, it is capable of spotting active fires as well as evidence of burn scars. The TRMM/VIRS 4-km^2 Fire Product shows the number of 4.4 km^2 pixels in each half-degree grid cell (each cell is 2500 square kilometres at the equator) that are hot enough to contain a large fire.

3 Horizontal distribution of tropospheric trace gases in the TTL

3.1 Satellite observations

The ODIN N_2O field at 17 km in MAM 2002–2004 and the MLS N_2O field at 100 hPa (~16.6 km in the tropics) for MAM 2005 are displayed in Figs. 1a and b, respectively. The HALOE CH_4 field at 17 km for 2002–2004 is shown in Fig. 2. The MOPITT CO field at 150 hPa (~14.3 km) in 2002–2004 together with the MLS CO fields at 100 and 150 hPa in 2005 are displayed in Figs. 3a–c, respectively. The N_2O fields at 17 km

(∼94 hPa) and at 100 hPa show a long band of enhanced concentration between 10° S–10° N extending from South America to South-East Asia with a pronounced maximum (>312 ppbv) over Africa and an extra-tropical maximum over Northern India. The CH_4 field at 17 km also displays a maximum over Africa (>1.66 ppmv) and a secondary one over South-East Asia. Finally, the CO fields at 150 hPa also show maximum concentration areas over Africa (>130 ppbv), South America, South-East Asia and the North-Western Pacific, still present at 100 hPa but of significantly reduced amplitude (78 ppbv). Note that in the extra-tropics at 150 hPa, the nadir-viewing MOPITT instrument is sensitive to the upper troposphere whilst the limb-viewing MLS instrument has a sensitivity peaking in the lower stratosphere. This explains the high amounts of CO measured by MOPITT in the Northern Hemisphere mid-latitudes and not observed by MLS.

In summary, all gases show significant longitudinal gradients with a maximum value primarily over Africa and, depending on the species, secondary more or less pronounced maxima above northern South America and South-East Asia. The Maritime continent in the Western Pacific never appears as a source region for the stratosphere.

3.2 Relation between trace gases and convection

Figure 4 displays the average OLR during the MAM 2002–2004 period derived from AVHRR while Fig. 5 shows the average meteorological parameters relevant to convection in the tropics from ECMWF analysis: a) temperature at 17 km (∼94 hPa), b) potential temperature at the same altitude level, c) height of the 370 K surface, roughly the tropopause, and d) horizontal wind at 17 km. During the MAM season, areas of low OLR (<236 $W\,m^{-2}$), shown by red lines in Fig. 4, representative of convection in the tropical middle troposphere, are located primarily over the Western Pacific (Micronesia), South-East Asia, Equatorial Africa and South America. The thin tongues of low OLR over the Atlantic and the Eastern Pacific corresponds to the Inter Tropical Convergence Zone (ITCZ). The very low OLR values (<220 $W\,m^{-2}$), shown by white lines in Fig. 4, indicative of cloud-top altitude in the tropical upper troposphere are lo-

cated over 4 areas: northern South America, Equatorial Africa, South-East Asia and the Western Pacific. Note that the longitudinal distribution of OLR is an indicator of the temperature of the cloud top and of the frequency of occurrence of convective clouds rather than a straight relationship with the cloud top height (Sherwood et al., 2004). In contrast to the OLR picture, the 6-year (1998–2003) TRMM radar measurements (Liu and Zipser, 2005) reveal that the maximum areas of OPF frequency above 14 km altitude are located first over Equatorial Africa and, to a lesser extent, over South America and Indonesia, but not over the Western Pacific. As pointed out by Alcala and Dessler (2002), continental convection is more efficient than oceanic convection for overshootings to reach the TTL, though, part of the disagreement between the OLR and OPF pictures could come from the strong diurnal modulation of land convection more developed in the afternoon, compared to the small amplitude of diurnal cycle of oceanic convection (Liu and Zipser, 2005).

According to the ECMWF analysis (Fig. 5), the average temperature at 17 km (94 hPa, 370 K potential temperature) is about 191±2 K. The coldest area (<191 K) is elongated along the Equator with two local minima (<190 K) over Africa and the Western Pacific. In contrast, the potential temperature at 17 km displays lower values above oceanic areas, particularly above Micronesia (<365 K), and two marked local maxima (370–375 K) above South America and Africa. The tropopause is higher and colder above the Western Pacific (~17.3 km; ~187.7 K) and Indonesia (~17.2 km; ~189.0 K) than above Equatorial Africa (~16.9 km; 189.2 K) and South America (~17.0 km; 190.0 K). Two convection regimes are identified: i) the first corresponds to an OLR minimum coinciding with a lifted and colder tropopause above the Western Pacific, and ii) the second corresponds to an OLR minimum over continents where the TRMM overshooting frequency maximum above 380 K and up to 420 K is reported (Liu and Zipser, 2005).

The trace gas distributions in the TTL (Figs. 1–3) match very well with this picture indicating that fast overshooting over land tropical convective systems is the predominant mechanism of troposphere-stratosphere exchange at global scale. In addition, the

highest N_2O, CH_4 and CO amounts are well confined inside the tropical zone by the Subtropical Westerly Jets (SWJ), with a local maximum in the extra-tropics over Northern India where the SWJ is displaced northward (Fig. 5). Furthermore, westerlies from America and easterlies from Africa bring high amounts of N_2O, CH_4 and CO contained in the convective zone above the Atlantic Ocean. However, there are also significant differences in the observed concentrations of the long-lived species between the continents. Possible explanations for these have been explored by simulations using a CTM model.

4 Model simulations

4.1 The MOCAGE-Climat model

MOCAGE-Climat (Teyssèdre et al., 2007[2]) is the climate version of Météo-France's tropospheric-stratospheric 3-D CTM MOCAGE. MOCAGE covers a range of scientific applications, from the study of climate-chemistry interactions to chemical data assimilation and 'chemical weather' forecasting. The MOCAGE model can use different horizontal resolutions with semi-Lagrangian advection scheme (Josse et al., 2004) and parameterizations for physical processes such as convection (Bechtold et al., 2001) and surface processes (Michou et al., 2004). The climate version used in the present study covers both the troposphere and the stratosphere, with 60 layers from the surface up to 0.07 hPa, and uses a Gaussian T21 ($5.8^\circ \times 5.8^\circ$) horizontal grid. The meteorological forcings from ECMWF constrain the model from 1 January 2000 to 31 December 2005, relying on 6-hourly operational analyses of winds, temperature and specific humidity.

[2]Teyssèdre, H., Michou, M., Chéroux, F., Clark, H. L., Dufour, A., Josse, B., Karcher, F., Olivié, D., Peuch, V.-H., St-Martin, D., Cariolle, D., Attié, J.-L., and Ricaud, P.: The climatic version of the MOCAGE tropospheric-stratospheric Chemistry and Transport Model: description, evaluation and sensitivity to surface processes, Atmos. Chem. Phys. Discuss., in preparation, 2007.

Chemistry used within MOCAGE-Climat is a combination of tropospheric (Crassier et al., 2000) and stratospheric (Lefèvre et al., 1994) chemical schemes, taking into account 83 species and 242 chemical reactions. Initial chemical conditions are taken from a previous simulation (WMO, 1998) to allow the model to quickly reach its numerical equilibrium, especially for long-lived species, such as N_2O and CH_4. Surface emissions prescribed in MOCAGE-Climat are based upon yearly- or monthly-averaged climatologies. The N_2O surface emissions are taken from the Global Emissions Inventory Activity and are climatologies representative of the year 1990 (Bouwman et al., 1995). They include anthropogenic and biogenic sources, for a total emission rate of 14.7 Tg(N) yr^{-1}. The CH_4 surface emissions are split into anthropogenic sources from the Intergovernmental Panel on Climate Change (Dentener et al., 2005), biomass burning (van de Werf et al., 2003) and biogenic sources (Michou and Peuch, 2002). The CH_4 climatologies are representative of the year 2000 for a total emission rate of 534 Tg(CH_4) yr^{-1}. The CO surface emissions are split into anthropogenic (including biomass burning) sources from Dentener et al. (2005) and biogenic sources as prescribed in the MOZART CTM (L. Emmons and J.-F. Lamarque, private communication). The CO climatologies are representative of the year 2000, for a total emission rate of 1122 Tg(CO) yr^{-1}. For more information on surface emissions, the reader should refer to Dentener et al. (2005). Finally, MOCAGE-Climat provides a comprehensive description of the chemical processes in the planetary boundary layer, free troposphere and stratosphere, adapted to the processes studied here.

4.2 Results of simulations

The N_2O distribution calculated by MOCAGE at 15 and 17 km for the MAM season in 2002–2004 averaged within bins of 10° in latitude and 30° in longitude, are shown in Fig. 6 together with the N_2O vertical net flux across the 150- and 100-hPa surfaces where positive (negative) values mean upward (downward) fluxes. The CH_4 and CO distributions at the same levels are shown in Fig. 7. At 15 km, N_2O shows a marked maximum over Equatorial Africa, extending from South America to South-East Asia. At

17 km, the maximum is still present over Africa, but the N_2O distribution is more zonally-symmetric being bounded by the SWJ (Fig. 5). The CH_4 fields are very similar, with a local minimum over the Eastern Pacific at 15 km. The CO distribution also shows similar features, i.e. maximum concentration over Africa, secondary maximum over South-East Asia and the Indian Ocean, with a marked minimum over South America at 17 km. The CO longitudinal gradients are much more contrasted than the N_2O and CH_4 gradients.

Although the simulations are roughly consistent with the observations, showing a maximum over Africa, particularly for CO and N_2O (correlation 0.8 and 0.7, respectively), but much less for CH_4 (correlation 0.4), there are also significant differences: i) the absence in the calculations of a relative maximum concentration of all species over South America, as present in the observations, and ii) the relatively higher concentration of tropospheric species at 17 km over Western Pacific, not present in the observations. This is explained by the map of net vertical N_2O flux. Indeed, the vertical flux of N_2O across the 150- and 100-hPa pressure surfaces is very consistent with the OLR distribution showing upward fluxes in area of low OLR (convective areas and ITCZ) and downward fluxes in the extra-tropics, except over South America where an area of subsidence is calculated but not supported by observations. The strongest vertical upward transport calculated over the Western Pacific is in very good agreement with the location of the lowest OLRs, but this feature is again not supported by the observations. Apparently, the associated convection does not bring air masses deeply enough into the TTL in agreement with Nessbit et al. (2000). A number of other significant differences can be seen in the model: i) the weaker North-South asymmetry, ii) the absence of N_2O maximum at 17 km over Northern India, and iii) the absence of relative minima of concentration of all species in the centre of the Indian Ocean (10°S, 75° E). But most importantly is the overall weaker contrast at 17 km between land and oceanic modelled concentrations of ~2 ppbv instead of ~15 ppbv for N_2O, ~0.03 ppmv instead of 0.15 ppmv for CH_4 and ~10 ppbv instead of ~25 ppbv for CO. Several processes could contribute to this underestimation: i) the broad horizontal resolution of

the model (5.8°×5.8°) that undoubtedly misrepresents subgrid convective processes, ii) the convection parameterization that does not produce overshootings significantly high, rapid and intense enough for penetrating the lower stratosphere, and iii) the too weak intensity of the local sources.

4.3 Distribution of sources at the surface and convection intensity in the model

Although the broad horizontal resolution of the model could contribute, most sensitive uncertainties in the calculations could come from an inadequate distribution of trace gas sources at the surface and an underestimation of the vertical transport across the tropopause. Figure 8 shows the average CO concentration distribution in MAM 2002–2004 reported by MOPITT at 850 hPa and calculated by MOCAGE at 1 km, the fire counts of TRMM/VIRS, and the ECMWF wind field at 1 km altitude. As shown by MOPITT and VIRS, the CO sources are mainly related to biomass burning in the tropics and anthropogenic production in northern mid-latitude populated regions. In the tropics, because of the high precipitations in convective regions, biomass-burning areas traced by fire counts are located at the edges of them only, while the emitted CO is further transported by surface winds into convergence zones. A maximum concentration is observed over the southern part of West Africa, secondary maxima over northern South-America, India and South-East Asia, and, as expected, a deep minimum over the West Pacific where there is no CO source. The enhancement of CO over the Atlantic Ocean comes from Africa via Easterly winds in the ITCZ. The MOCAGE CO distribution at 1 km is quite consistent with this picture in the tropics, displaying high amounts (>130 ppbv) over Africa, northern South America and South-East Asia. At mid-latitude, the strong CO sources in Asia are well captured. Those of Northern America and Europe are strongly underestimated, but this will have little impact on the TTL since they are far from tropical convective regions.

Figure 9 shows the longitude-altitude cross-section of CO, CH_4, and N_2O from MOCAGE in MAM 2002-2004 within the latitude band 10° S–10° N, together with a schematic representation of the horizontal and vertical transports. Superimposed on

the cross-sections is the average OLR for MAM 2002-2004 in the same latitude band, showing OLR minima over South America (60–80° W), Equatorial Africa (10–30° E), Indonesia (∼100° E) and the Western Pacific (∼160° E). CO uplifts can be seen over the three CO rich convective regions, resulting in maxima between 10 and 15 km, particularly intense over Africa. Because of its shorter lifetime, CO is little mixed horizontally in the mid- and upper troposphere, showing strong contrast between subsident and adjacent convective regions. However, contrarily to the observations, the contrast vanishes in the tropopause region. The model underestimates the altitude reached by the convective updrafts over land. The CH_4 distribution at the surface in the tropics mainly associated to wetlands and to a smaller part (10%) to biomass burning, shows maximum concentrations over Africa and a less intense maximum over South-East Asia, but a minimum over South America and the Eastern Pacific. MOCAGE CH_4 fields over northern South America are much weaker than the CH_4 concentrations from the measurements of the satellite-borne SCanning Imaging Absorption SpectroMeter for Atmospheric CHartographY (SCIAMACHY) instrument as reported in Frankenberg et al. (2006) over the MAM period. Nevertheless, MOCAGE results are in overall agreement with the results from the CTM TM4 (Frankenberg et al., 2006) using 155 $Tg(CH_4)$ yr^{-1} CH_4 emission for wetlands compared to 160 $Tg(CH_4)$ yr^{-1} in MOCAGE. This indeed may indicate a systematic underestimation of CH_4 emissions by evergreen forests not included in models, which could also apply to Africa and to some degree to Indonesia and South-East Asia. As for CO, CH_4 is lifted by convection resulting in concentration maxima around 10–15 km above Africa and South-East Asia. But since the CH_4 lifetime is much longer, the gas is better mixed in the troposphere, showing only a minimum in the subsident area over the Eastern Pacific. However, as for CO, the signature of convective lifting decreases rapidly in the tropopause region. At 17 km, the contrast between maximum and minimum concentrations is only 0.03 ppmv where satellite measurements are reporting 0.15 ppmv. Again at these levels, the impact of convective transport is significantly underestimated in the model. Finally the long-lived N_2O shows slightly depleted amounts at surface levels in the tropics compared to the

mid-troposphere. The additional N_2O sources due to agricultural activities are outside the equatorial belt. A maximum of 320 ppbv is observed between 10 and 15 km over Africa compared to an average concentration of 316 ppmv within this layer. The contrast reduces to 2 ppbv in the tropopause region compared to the 15 ppbv observed. The penetration of N_2O-rich tropospheric air masses in the stratosphere is also largely underestimated in the model.

The slightly depleted amounts of surface N_2O and, to a lesser extent, of surface CH_4 (whilst not present in surface CO) can be explained by the net negative budget between loss induced by convective uplift and production from surface emission. Indeed, from surface emission rates inserted in the model, injection of molecules at a given grid point is very fast for CO (~100 molecules m^{-2} s^{-1}), intermediate for CH_4 (~1–10 molecules m^{-2} s^{-1}), but very slow for N_2O (<1 molecule m^{-2} s^{-1}). Consequently, convective uplifts locally deplete surface N_2O and, to a lesser extent, surface CH_4, but does not significantly affect surface CO. Furthermore, as illustrated by vertical profiles obtained by Josse et al. (2004), convective upward fluxes in MOCAGE are somewhat more intense when calculated from the parameterization of Bechtold et al. (2001) than that of Tiedtke (1989).

The upper tropospheric and, particularly, the TTL distributions of these three long-lived species show an elongated maximum from South America to Indonesia peaking above Africa (clearly visible in the CH_4 field). Indeed, together with the rapid uplift over convective areas, the horizontal transport continuously re-distributes constituents along the longitude. This is true in the stratosphere but also at the top of the TTL. The Easterly Jet is present from the Western Pacific to Africa reaching the middle of the Atlantic Ocean, while the Westerly Jet develops from the Western Pacific to South America reaching the middle of the Atlantic Ocean. This explains the maxima of constituents spreading apart from the centre of the convective areas, towards the Atlantic Ocean and the Indian Ocean.

Overall, and although there are obvious misrepresentations of some of the sources, i.e. CH_4 emissions by evergreen forests, MOCAGE-Climat captures quite well the loca-

tion of the convective lifting of the species emitted at the surface, but underestimates significantly its amplitude, that is the altitude levels reached by the vertical convective transport. Thus, the main reason for the large discrepancies between model and observations of the horizontal distribution of the species in the TTL at 17 km appears to be the misrepresentation of the maximum height reached by convective transport over land in MOCAGE.

5 Concluding remarks

The average horizontal distribution of N_2O, CH_4 and CO in the tropical tropopause layer at 17 km during the March–April–May season has been investigated from the space-borne measurements of the ODIN/SMR, the UARS/HALOE and the TERRA/MOPITT instruments in 2002–2004, completed by recent observations of the space-borne AURA/MLS instrument during the same season in 2005.

All gases show significant longitudinal gradients with maximum amounts primarily over Africa and, depending on the species, secondary more or less pronounced maxima above northern South America and South-East Asia. The Maritime continent in the Western Pacific never appears as a source region for the stratosphere. The existence of large longitudinal gradients at a latitude circle where the circulation is essentially zonal, strongly supports the concept of a larger contribution of fast convective updraft compared to slow ascent by radiative heating, to the troposphere-stratosphere exchange at global scale. Furthermore, the co-location of the maximum tropospheric trace gas concentrations with the overshooting features reported by the TRMM satellite precipitation radar, indicates that the process responsible is the fast and intense diurnal convection developing over land areas.

Calculations carried out with the MOCAGE-Climat CTM well capture the location of the maximum gas concentration but of lesser amplitude. Although there are obvious misrepresentations of some of the sources in the model, i.e. CH_4 emissions by evergreen forests, the main reason for discrepancy appears to be the underestimation of

the maximum height reached by land convective transport in MOCAGE.

Acknowledgements. We would like to thank our colleagues from the Odin and the NCAR MOPITT teams, and M. Michou at CNRM (France) for helpful comments on MOCAGE-Climat. Odin is a Swedish-led satellite project funded jointly by the Swedish National Space Board (SNSB), the Canadian Space Agency (CSA), the National Technology Agency of Finland (Tekes), and the Centre National d'Etudes Spatiales (CNES). Odin data V222 are stored in the Ether French atmospheric data base (http://ether.ipsl.jussieu.fr). Aspects of the research described in this paper carried out by the Jet Propulsion Laboratory, California Institute of Technology, was under a contract with the National Aeronautics and Space Administration. This project has been funded in France by the Programme National de Chimie Atmosphérique (PNCA). BB has been funded by the European Integrated Project SCOUT-O3. Interpolated OLR data are provided by the NOAA-CIRES ESRL/PSD Climate Diagnostics branch, Boulder, Colorado, USA, from their Web site at http://www.cdc.noaa.gov/. The TRMM/VIRS data used in this study were acquired as part of the NASA's Earth-Sun System Division and archived and distributed by the Goddard Earth Sciences (GES) Data and Information Services Centre (DISC) Distributed Active Archive Centre (DAAC).

References

Alcala, C. M. and Dessler, A. E.: Observations of deep convection in the tropics using the TRMM precipitation radar, J. Geophys. Res., 107(D24), 4792, doi:10.129/2002JD002457, 2002.

Barret, B., De Mazière, M., and Mahieu, E.: Ground-based FTIR measurements of CO from the Jungfraujoch: characterisation and comparison with in situ surface and MOPITT data, Atmos. Chem. Phys., 3, 2217–2223, 2003, http://www.atmos-chem-phys.net/3/2217/2003/.

Barret, B., Ricaud, P., Santee, M. L., et al.: Intercomparisons of trace gases profiles from the Odin/SMR and Aura/MLS limb sounders, J. Geophys. Res., 111, D21302, doi:10.1029/2006JD007305, 2006.

Bechtold, P., Bazile, E., Guichard, F., Mascart, P., and Richard, E.: A mass flux convection scheme for regional and global models, Quart. J. Roy. Meteor. Soc., 127, 869–886, 2001.

Bouwman, A. F., Van der Hoek, K. W., and Olivier, J. G. J.: Uncertainties in the global source distribution of nitrous oxide, J. Geophys. Res., 100(D2), 2785–2800, 1995.

Brasseur, G., P., Orlando, J. J., and Tyndall, G. S.: Atmospheric chemistry and global change, 2nd edition, Oxford University Press, New York, Oxford, ISBN-0-19-510521-4, 1999.

Christian, H. J., Blakeslee, R. J., Boccippio, D. J., et al.: Global frequency and distribution of lightning as observed from space by the Optical Transient Detector, J. Geophys. Res., 108(D1), 4005, doi:10.1029/2002JD002347, 2003.

Crassier, V., Suhre, K., Tulet, P., and Rosset, R.: Developement of a reduced chemical scheme for use in mesoscale meteorological models, Atm. Env., 34, 2633–2644, 2000.

Danielsen, E. F.: A dehydration mechanism for the stratosphere, Geophys. Res. Lett., 9, 605–608, 1982.

Danielsen, E. F.: In situ evidence of rapid, vertical, irreversible transport of lower tropospheric air into the lower stratosphere by convective cloud turrets and by large scale up welling in tropical cyclones, J. Geophys. Res, 98, 8665–8681, 1993.

Deeter, M. N., Emmons, L. K., Edwards, D. P., Gille, J. C., and Drummond, J. R.: Vertical resolution and information content of CO profiles retrieved by MOPITT, Geophys. Res. Lett., 31, L15112, doi:10.1029/2004GL020235, 2004.

Dentener, F., Stevenson, D., Cofala, J., Mechler, R., Amann, M., Bergamaschi, P., Raes, F., and Derwent, R.: The impact of air pollutant and methane emission controls on tropospheric ozone and radiative forcing: CTM calculations for the period 1990–2030, Atmos. Chem. Phys., 5, 1731–1755, 2005, http://www.atmos-chem-phys.net/5/1731/2005/.

Drummond, J. R. and Mand, G. S.: The Measurements of Pollution in the Troposphere (MOPITT) instrument: Overall performance and calibration requirements, J. Atmos. Oceanic Technol., 13, 314–320, 1996.

Emmons, L. K., Deeter, M. N., Gille, J. C., et al.: Validation of MOPITT CO retrievals with aircraft in situ profiles, J. Geophys. Res., 109, D03309, doi:10.1029/2003JD004101, 2004.

Filipiak, M. J., Harwood, R. S., Jiang, J. H., Li, Q., Livesey, N. J., Manney, G. L., Read, W. G., Schwartz, M. J., Waters, J. W., and Wu, D. L.: Carbon monoxide measured by the EOS Microwave Limb Sounder on Aura: First results, Geophys. Res. Lett.,32, L14825, doi:10.1029/2005GL022765, 2005.

Folkins, I., Bernath, P., Boone, C., Lesins, G., Livesey, N. Thompson,, A. M., Walker, K., and Witte, J. C.: Seasonal cycles of O_3, CO, and convective outflow at the tropical tropopause,

Geophys. Res. Lett., 33, L16802, doi:10.1029/2006GL026602, 2006.
Frankenberg, C., Meirink, J. F., Bergamaschi, P., Goede, A. P. H., Heimann, M., Körner, S., Platt, U., van Weele, M., and Wagner, T.: Satellite chartography of atmospheric methane from SCIAMACHY on board ENVISAT: Analysis of the years 2003 and 2004, J. Geophys. Res., 111, D07303, doi:10.1029/2005JD006235, 2006.
Frisk, U., Hagström, M., Ala-Laurinaho, J., et al.: The Odin satellite I: Radiometer design and test, Astron. Astrophys., 402(3), L27–L34, doi:10.1051/0004-6361:20030335, 2003.
Froidevaux, L., Liversey, N. J., Read, W. G., et al.: Early validation analyses of atmospheric profiles from EOS MLS on the Aura satellite, IEEE Trans. Geosci. Remote Sensing, 44(5), 1106–1121, 2006.
Giglio, G., Kendall, J. D., and Tucker, C. J.: Remote sensing of fires with the TRMM VIRS, Int. J. Remote Sens., 21, 203–207, 2000.
Heald, C. L., Jacob, D. J., Palmer, P. I., Evans, M. J., Sachse, G. W., Singh, H. B., and Blake, D. R.: Biomass burning emission inventory with daily resolution: Application to aircraft observations of Asian outflow, J. Geophys. Res., 108(D21), 8811, doi:10.1029/2002JD003082, 2003.
Holton, J. R., Haynes, P. H., Douglass, A. R., Rood, R. B., and Pfister, L.: Stratosphere-troposphere exchange, Rev. Geophys., 33, 403–439, 1995.
Josse, B., Simon, P., and Peuch, V.-H.: Rn-222 global simulations with the multiscale CTM MOCAGE, Tellus, 56B, 339–356, 2004.
Lefèvre, F., Brasseur, G. P., Folkins, I., Smith, A. K., and Simon, P.: Chemistry of the 1991-1992 stratospheric winter: Three-dimensional model simulations, J. Geophys. Res., 99, 9183–8195, 1994.
Levine, J. G., Braesicke, P., Harris, N. R. P., Savage, N. H. and Pyle, J.: Pathways and Timescales for Troposphere-to-Stratosphere Transport via the Tropical Tropopause Layer and their Relevance for Very Short Lived Substances, J. Geophys. Res., 112, D04308, doi:10.1029/2005JD006940, 2007.
Li., Q., Jiang, J. H., Wu, D. L., et al.: Convective outflow of South Asia pollution: A global CTM simulation compared with EOS MLS observations, Geophys. Res. Lett., 32, L14826, doi:10.1029/2005GL022762, 2005.
Liebmann, B., and Smith, C. A.: Description of a Complete (Interpolated) Outgoing Longwave Radiation Dataset, Bull. Am. Meteorol. Soc., 77, 1275–1277, 1996.
Livesey, N. J., Read, W. G., Filipiak, M. J., et al.: Earth Observing System (EOS) Mi-

crowave Limb Sounder (MLS), Version 1.5 Level 2 data quality and description document, Jet Propulsion Laboratory, Tech. Rep., D-32381, 2005; available on the MLS website, http://mls.jpl.nasa.gov.
Livesey, N. J., Van Snyder, W., Read, W. G., and Wagner, P. A.: Retrieval algorithms for the EOS Microwave Limb Sounder (MLS) instrument, IEEE Trans. Geosci. Remote Sens., 44(5), 1144–1155, 2006.
Liu, C., and Zipser, E. J.: Global distribution of convection penetrating the tropical tropopause, J. Geophys. Res., 110, D23104, doi:10.1029/2005JD006063, 2005.
Michou, M., and Peuch, V.-H.: Surface exchanges in the MOCAGE multiscale Chemistry and Transport Model, J. Water Sci., 15, 173–203, 2002.
Michou, M., Laville, P., Sera, D., et al.: Measured and modeled dry deposition velocities over the ESCOMPTE area, Atmos. Res., 74, 89–116, doi:10;1016/j.atmosres.2004.04.011, 2004.
Murtagh, D., Frisk, U., Merino, F., et al.: An overview of the Odin atmospheric mission, Can. J. Phys., 80, 309–319, 2002.
Nesbitt, S. W., Zipser, E. J., and Cécil, D. J.: A census of precipitation features in the tropics using TRMM: Radar, ice scattering, and lightning observations, J. Clim., 13, 4087–4106, 2000.
Park, M., Randel, W. J., Kinnison, D. E., Garcia, R. R., Choi, W.: Seasonal variation of methane, water vapor, and nitrogen oxides near the tropopause: Satellite observations and model simulations, J. Geophys. Res., 109, D03302, doi:10.1029/2003JD003706, 2004.
Pommereau, J. P., Garnier, A., Held, G., Gomes, A.-M., Goutail, F., et al.: An overview of the HIBISCUS campaign, Atmos. Chem. Phys. Discuss., 7, 2389–2475, 2007, http://www.atmos-chem-phys-discuss.net/7/2389/2007/.
Rodgers, C. D.: Inverse methods for atmospheric sounding: theory and practice, 1st ed., World Sci., River Edge, N. J., 2000.
Russell III, J. M., Gordley, L. L., Park, J. H., et al.: The Halogen Occultation Experiment, J. Geophys. Res., 98, 10 777–10 797, 1993.
Schoeberl, M. R., Duncan, B. N., Douglass, A. R., Waters, J., Livesey, N., Read, W., and Filipiak, M.: The carbon monoxide tape recorder, Geophys. Res. Lett., 33, L12811, doi:10.1029/2006GL026178, 2006.
Sherwood, S. C. and Dessler, A. E.: On the control of stratospheric humidity, Geophys. Res. Lett., 27(16), 2513–2516, doi:10.1029/2000GL011438, 2000.
Sherwood, S. C., Chae, J.-H., Minnis, P., and McGill, M.: Underestimation of

deep convective cloud tops by thermal imagery, Geophys. Res. Lett., 31, L11102, doi:10.1029/2004GL019699, 2004.
Tiedtke, M.: A comprehensive mass flux scheme for cumulus parametrization in large scale models, Mon. Wea. Rev., 117, 1779–1800, 1989.
Urban, J., Lautié, N., Le Flochmoën, E., et al.: Odin/SMR limb observations of stratospheric trace gases: Validation of N_2O, J. Geophys. Res., 110, D09301, doi:10.1029/2004JD005394, 2005.
van der Werf, G. R., Randerson, J. T., Collatz, G. J., and Giglio, L.: Carbon emissions from fires in tropical and subtropical ecosystems, Global Change Biol., 9, 547–562, 2003.
Waters, J. W., Froidevaux, L., and Harwood, R. S.: The Earth Observing System Microwave Limb Sounder (EOS MLS) on the Aura satellite, IEEE Trans. Geosci. Remote Sensing, 44(5), 1075–1092, 2006.
World Meteorological Organization, Scientific assessment of ozone depletion: 1998, Rep. 44, Geneva, Switzerland, 1998.

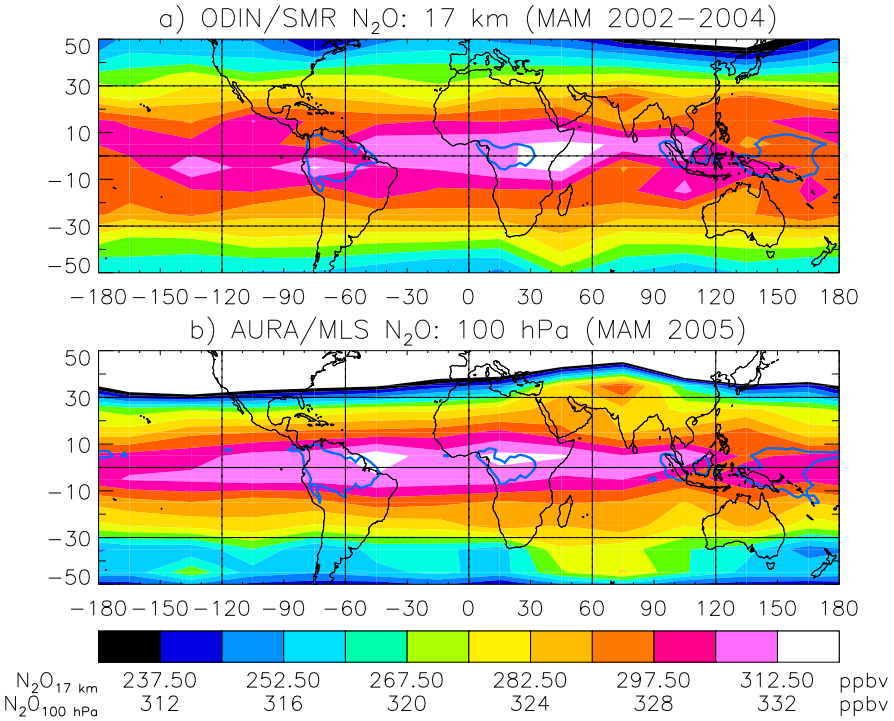

Fig. 1. Nitrous oxide (N_2O) fields at 17 km observed **(a)** by ODIN/SMR in MAM 2002–2004 and **(b)** by AURA/MLS at 100 hPa (~16.6 km in the tropics) in MAM 2005. The blue line is the 220 W m^{-2} OLR isoline.

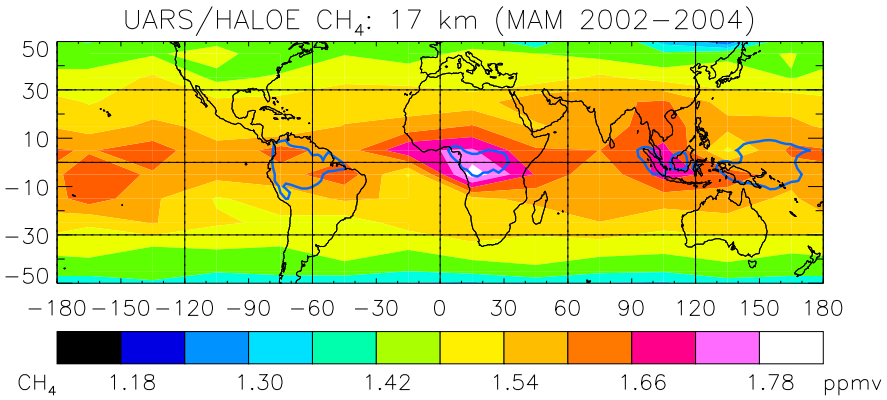

Fig. 2. Methane (CH_4) field at 17 km in MAM 2002-2004 from UARS/HALOE. The blue line is the 220 W m^{-2} OLR isoline.

ACPD
7, 3269–3300, 2007

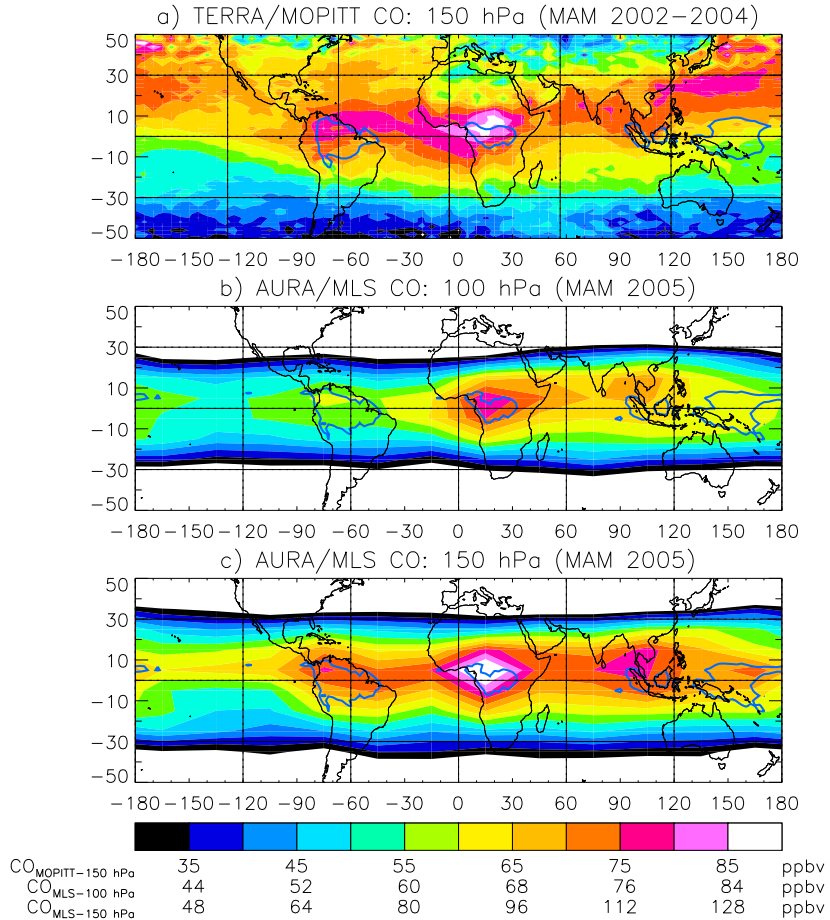

Fig. 3. Carbon monoxide (CO) fields **(a)** at 150 hPa (~14.3 km) in MAM 2002–2004 from TERRA/MOPITT and **(b)** at 100 hPa and **(c)** at 150 hPa in MAM 2005 from AURA/MLS. The blue line is the 220 W m^{-2} OLR isoline.

ACPD
7, 3269–3300, 2007

EGU

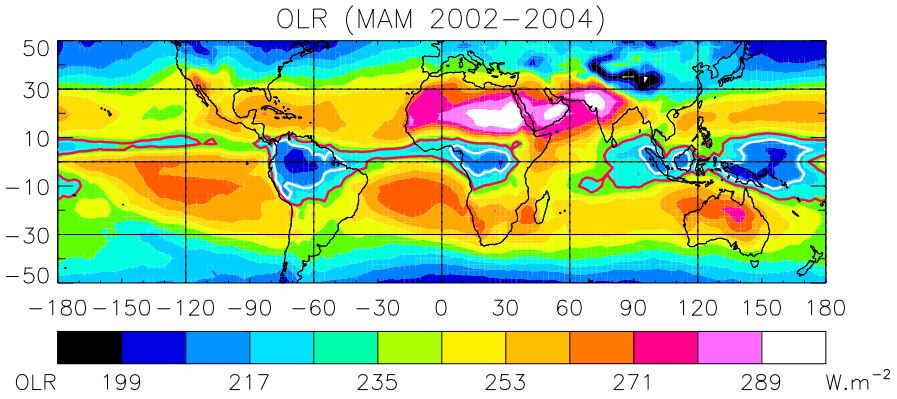

Fig. 4. Outgoing Longwave Radiation OLR (W m^{-2}) in MAM 2002–2004 from AVHRR. The red line is the 236 W m^{-2} isoline and the white line the 220 W m^{-2}.

ACPD
7, 3269–3300, 2007

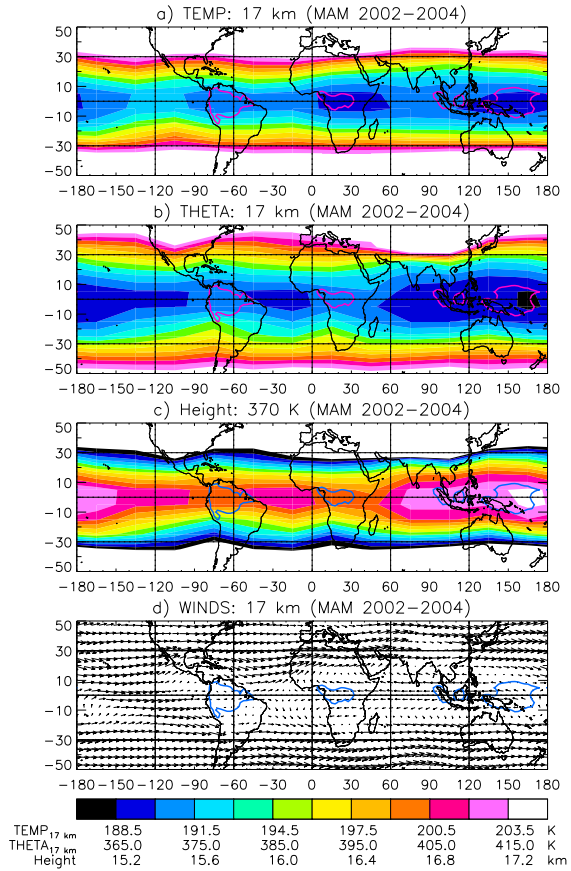

Fig. 5. Fields of **(a)** ECMWF temperature at 17 km, **(b)** potential temperature at 17 km, **(c)** altitude of the 370-K surface, approximately the tropopause, and **(d)** ECMWF horizontal winds at 17 km, all averaged during the MAM 2002–2004 period. The blue and red lines are the 220 W m^{-2} OLR isoline.

ACPD
7, 3269–3300, 2007

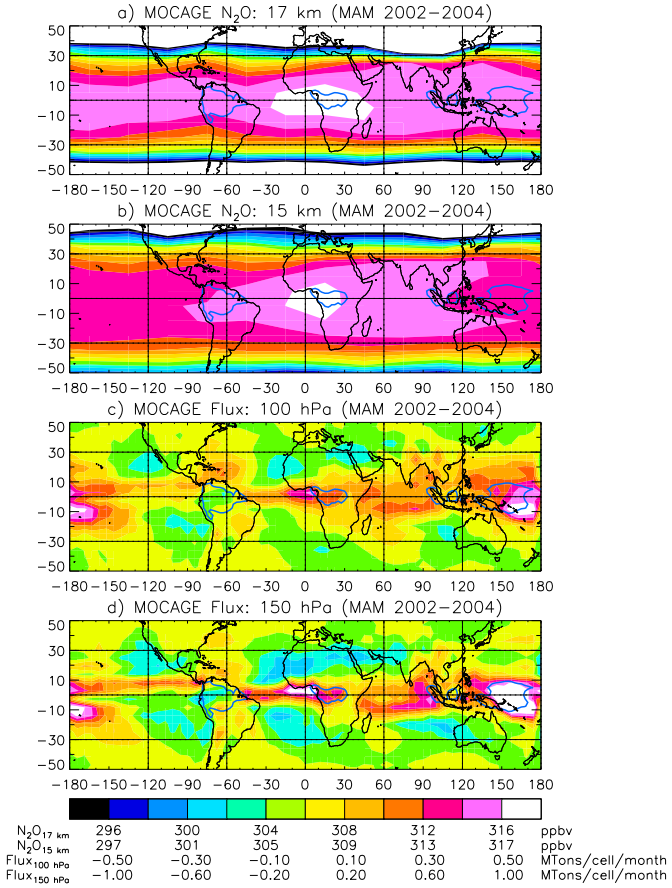

Fig. 6. Nitrous oxide (N_2O) fields at **(a)** 17 km and **(b)** 15 km, and vertical fluxes across the surfaces of **(c)** 100 hPa and **(d)** 150 hPa, as calculated by MOCAGE in MAM 2002–2004. Positive (negative) fluxes represent upward (downward) transport. The blue line is the 220 W m^{-2} OLR isoline.

ACPD
7, 3269–3300, 2007

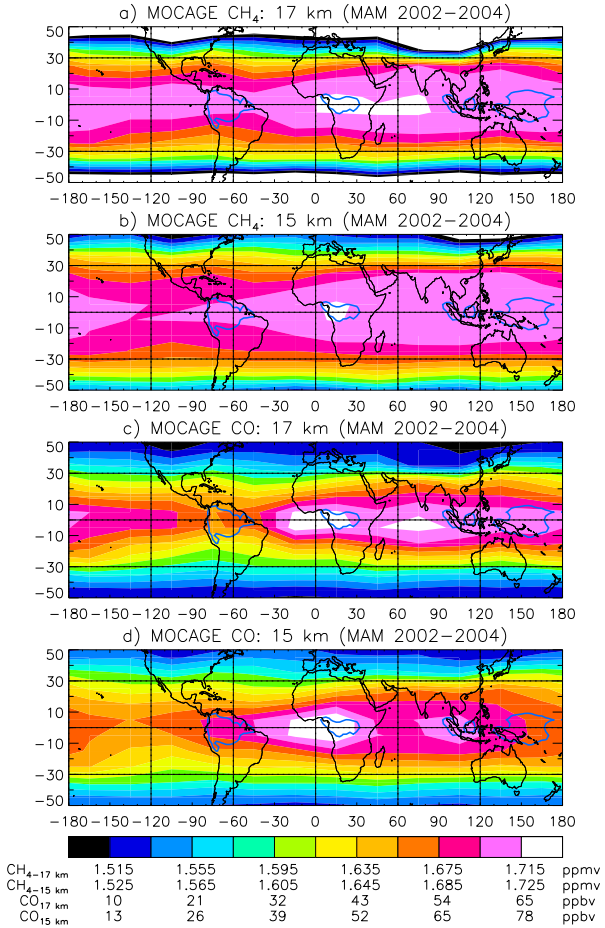

Fig. 7. Methane (CH_4) fields at **(a)** 17 km and **(b)** 15 km, and carbon monoxide (CO) fields at **(c)** 17 km and **(d)** 15 km as calculated by MOCAGE in MAM 2002–2004. The blue line is the 220 W m^{-2} OLR isoline.

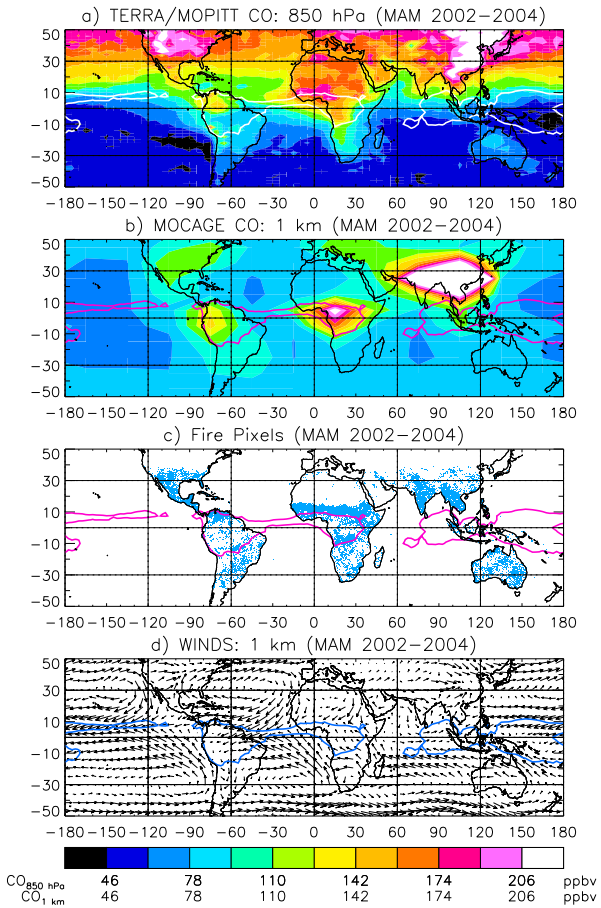

Fig. 8. Fields of carbon monoxide (CO) **(a)** as measured by TERRA/MOPITT at 850 hPa and **(b)** as calculated by MOCAGE at 1 km altitude, **(c)** TRMM/VIRS fire counts and **(d)** ECMWF wind field at 1 km height, all averaged during the MAM 2002–2004 period. The white, red and blue lines are the 236 W m^{-2} isolines.

ACPD
7, 3269–3300, 2007

EGU

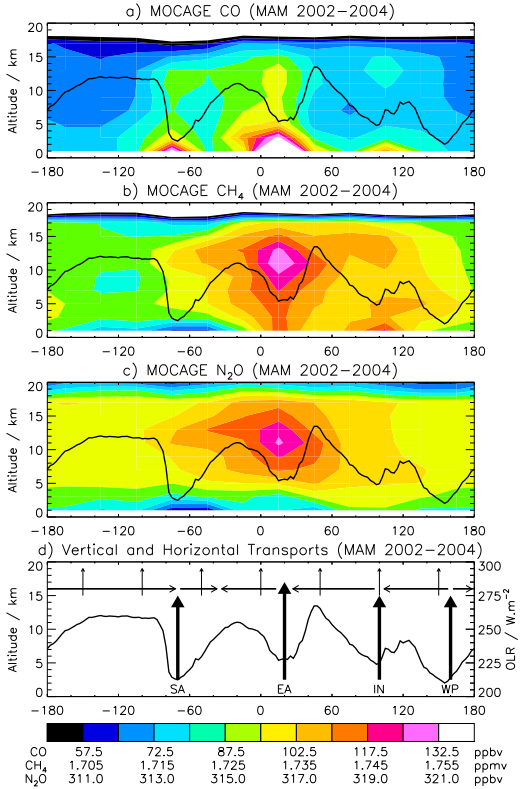

Fig. 9. Longitude-altitude cross-section (10° S–10° N) of **(a)** CO, **(b)** CH_4 and **(c)** N_2O, as calculated by MOCAGE during the MAM 2002–2004 period, and **(d)** schematic representation of the longitude vs. height equatorial (10° S–10° N) distributions of the vertical and horizontal transports. The black curve is the OLR longitudinal distribution within the 10° S–10° N latitude band averaged from 2002 to 2004 for the MAM period (right axis: minimum value is 200 W m^{-2}, maximum value is 300 W m^{-2}). (SA: South America, EA: Equatorial Africa, IN: Indonesia, and WP: Western Pacific).

ACPD
7, 3269–3300, 2007